At which time scale does the complementary principle perform best on evaporation estimation?

Liming Wang[1], Songjun Han[2], Fuqiang Tian[1*].

[1] Department of Hydraulic Engineering, State Key Laboratory of Hydroscience and Engineering, Tsinghua University, Beijing 100084, China

[2] State Key Laboratory of Simulation and Regulation of Water Cycle in River Basin, China Institute of Water Resources and Hydropower Research, Beijing 100038, China

Correspondence to:

Fuqiang Tian: tianfq@mail.tsinghua.edu.cn

1   **Abstract**

2   The complementary principle has been widely used to estimate evaporation under different

3   conditions. However, it remains unclear at which time scale the complementary principle

4   performs best. In this study, evaporation estimations were conducted at 88 eddy covariance

5   (EC) monitoring sites at multiple time scales (daily, weekly, monthly, and yearly) by using

6   sigmoid and polynomial generalized complementary functions. The results indicate that the

7   generalized complementary functions exhibit the highest skill in estimating evaporation at the

8   monthly scale. The uncertainty analysis shows that this conclusion is not affected by

9   ecosystem type or energy balance closure method. Through comparisons at multiple time

10   scales, we found that the slight difference between the two generalized complementary

11   functions only exists when the independent variable (x) in the functions approaches 1. The

12   results differ for the two models at daily and weekly scales. However, such differences vanish

13   at monthly and annual time scales with few high x values occurring. This study demonstrates

14   the applicability of generalized complementary functions across multiple time scales and

15   provides a reference for choosing a suitable timestep for evaporation estimations in relevant

16   studies.

17 **Keywords:**

18 Evaporation; Generalized complementary functions; Multiple time scales; Ecosystem types

19

1. Introduction

Terrestrial evaporation (E) including soil evaporation, wet canopy evaporation, and plant transpiration, is one of the most important components in the global water cycle and energy balance (Wang and Dickinson, 2012). The evaporation process affects the atmosphere through a series of feedbacks involving humidity, temperature, and momentum (Brubaker and Entekhabi, 1996; Neelin et al., 1987; Shukla and Mintz, 1982). Quantifying evaporation is crucial for a deep understanding of water and energy interactions between the land surface and the atmosphere. Generally, meteorological studies focus on evaporation changes at hourly and daily scales; hydrological applications require evaporation data at weekly, monthly or longer time scales (Morton, 1983); and climate change studies focus more on interannual variations. The observation of E can occur at different time scales. For example, the eddy covariance, lysimeter, and scintillometer can measure evaporation at the half-hour scale, and water balance methods can observe evaporation at monthly to yearly scales (Wang and Dickinson, 2012). However, in most situations, an observation is unavailable, and the estimation of E is necessary. There are several types of methods for evaporation estimations, for example, the Budyko-type methods (Budyko, 1974; Fu, 1981), the Penman-type methods (Penman, 1948; Monteith, 1965) and the complementary-type methods (Bouchet, 1963; Brutsaert and Stricker, 1979). The Budyko-type methods perform well at annual or longer time scales; the Penman-type methods can be applied at hourly and daily scales, while the complementary-type methods are used at multiple time scales (Crago and Crowley, 2005; Han and Tian, 2018; Crago and Crowley, 2018; Ma et al., 2019) without explicit consideration of the time scale issue.

43   Recently, the complementary principle, as one of the major types of E estimation methods,

44   has drawn increasing attention because it can be implemented with standard meteorological

45   data (radiation, wind speed, air temperature, and humidity) without complicated underlying

46   surface properties. Based on the coupling between the land surface and the atmosphere, the

47   complementary principle assumes that the limitation of the wetness state in the underlying

48   surface on evaporation can be synthetically reflected by atmospheric wetness (Han et al.,

49   2020). Bouchet (1963) first proposed the "complementary relationship" (CR), which

50   suggested that apparent potential evaporation (E_{pa}) and actual E depart from potential

51   evaporation (E_{po}) in equal absolute values but opposite directions ($E_{pa} - E_{po} = E_{po} - E$).

52   According to the Advection–Aridity approach (AA, Brutsaert and Stricker, 1979), E_{pa} is

53   formulated by Penman's (1948) equation (E_{pen}), and E_{po} is formulated by Priestley-Taylor's

54   (1972) equation (E_{PT}). Subsequently, the CR was extended to a linear function with an

55   asymmetric parameter (Brutsaert and Parlange, 1998). Further studies have found that the

56   linear function underestimates E in arid environments and overestimates E in wet

57   environments (Han et al., 2008; Hobbins et al., 2001; Qualls and Gultekin, 1997). To address

58   this issue, Han et al. (2011; 2012; 2018) proposed a sigmoid generalized complementary

59   function (SGC, see equation (1) for details). As a modification to the AA approach, the SGC

60   function illustrates the relationship between two dimensionless terms, E/E_{pen} and E_{rad}/E_{pen},

61   where E_{pen} is Penman evaporation (Penman, 1948) and E_{rad} is the radiation term of E_{pen}. The

62   SGC function shows higher accuracy in estimating E (Han and Tian, 2018; Ma et al., 2015b;

63   Zhou et al., 2020) and outperforms the linear functions, especially in dry desert regions and

64   wet farmlands (Han et al., 2012). Obtaining the impetus from Han et al. (2012), Brutsaert

65 (2015) proposed a quartic polynomial generalized complementary function (PGC, see

66 equation (5) for detail). The PGC function describes the relationship between E/E_{pa} and

67 E_{po}/E_{pa}, where E_{pa} and E_{po} are formulated in the manner of the AA approach. The PGC

68 function has also been frequently used in recent years (Brutsaert et al., 2017; Hu et al., 2018;

69 Liu et al., 2016; Zhang et al., 2017).

70

71 The prerequisite of the complementary principle is adequate feedback between the land

72 surface and the atmosphere, which results in an equilibrium state. In this situation, the

73 wetness condition of the land surface can be largely represented by the atmospheric

74 conditions. Therefore, the time scales used in the complementary principle need to satisfy the

75 adequate feedback assumption. However, this issue involves the complex processes of

76 atmospheric horizontal and vertical motion, and these processes are difficult to explain

77 theoretically. Morton (1983) noted this problem earlier and suggested that the complementary

78 principle is not suitable for short time scales (e.g., less than 3 days) mainly because of the

79 potential lag times associated with the response of energy and water vapor storage to

80 disturbances in the atmospheric boundary layer. However, there is no solid evidence or

81 theoretical identification to support this inference. The original complementary relationship

82 and the AA function are not limited by applicable time scales. In the derivation of the

83 advanced generalized complementary functions (SGC of Han and Tian (2018) and PGC of

84 Brutsaert (2015)), no specific time scale is defined. In practice, the complementary principle

85 has been widely adopted to estimate E at multiple time scales, including hourly (Crago and

86 Crowley, 2005; Parlange and Katul, 1992), daily (Han and Tian, 2018; Ma et al, 2015b),

87   monthly (Ma et al, 2019; Brutsaert, 2019), and annual scales (Hobbins et al., 2004). The

88   accuracy of the results have varied in different studies. Crago and Crowley (2005) found that

89   the linear complementary function performs well in estimating E at small time scales of less

90   than half-hour using the data from several well-known experimental projects (e.g.,

91   International Satellite Land Surface Climatology Project). The correlation coefficient

92   between simulated E and observed E ranges from 0.87 to 0.92 in different experiments. The

93   results of Ma et al. (2015b) indicated that the SGC function (Root-Mean-Square Error,

94   RMSE = 0.39 mm day^{-1}) performs well in estimating E in an alpine steppe region of the

95   Tibetan Plateau at the daily scale. Han and Tian (2018) applied the SGC function to the daily

96   data of 20 EC sites from FLUXNET and found that it performed well in estimating E with a

97   mean Nash‒Sutcliffe efficiency (NSE) value of 0.66. Crago and Qualls (2018) evaluated the

98   PGC function and their rescaled complementary functions using the weekly data of 7

99   FLUXNET sites in Australia, and the results showed that all the functions performed

100   adequately with a correlation coefficient between simulated E and observed E higher than

101   0.9. Ma et al. (2019) also validated an emendatory polynomial complementary function at the

102   monthly scale, and the NSE values of 13 EC sites in China were higher than 0.72. At the

103   annual scale, Zhou et al. (2020) found that the mean NSE of the SGC function was 0.28 for

104   15 catchments in the Loess Plateau. Since these results were derived with different functions

105   under varied conditions, it is difficult to determine at which time scale the performance is the

106   best, and it is more difficult to explain theoretically how long the land-atmosphere feedback

107   needs to achieve equilibrium.

108

109   In previous studies, the model validations were mostly completed at the daily scale

110   (Brutsaert, 2017; Han and Tian 2018; Wang et al. 2020), and the datasets of evaporation

111   estimation were often established at the monthly scale (Ma et al., 2019; Brutsaert et al.,

112   2019). However, each study only focused on a single timescale. In this study, we assessed the

113   performance of the complementary functions on evaporation estimation at multiple time

114   scales (daily, weekly, monthly, and yearly). The assessment was carried out at 88 EC

115   monitoring sites with > 5-year-long observation records. In view of the fact that the

116   complementary principle has developed to the nonlinear generalized forms, we selected two

117   nonlinear complementary functions in the literature, i.e., the SGC function (Han et al., 2012;

118   2018) and the PGC function (Brutsaert, 2015). The key parameters of the complementary

119   functions need to be determined by calibration. We chose the uniform database and the

120   uniform parameter calibration methods for the optimization of the two complementary

121   functions. We aimed to determine the most suitable timescale for the complementary

122   functions through a comparison of the performances at different timescales. It's important for

123   not only a deep understanding of the application of the complementary principle but also

124   timestep selection in evaporation database establishment and evaporation trend analysis.

125

126   This paper is organized as follows: Section 1 briefly describes the development of the

127   complementary theory and our motivations to investigate the timescale issue. Section 2

128   describes the two functions, the parameter calibration method, and the data sources and

129   processing. Section 3 shows and discusses the performance of the complementary functions

130   at multiple time scales, the dependence of the key parameters on time scales, and the

131   uncertainties in the analysis. The conclusions are given in Section 4.

132

133   **2. Methodology**

134   **2.1 Sigmoid generalized complementary function**

135   Han et al. (2012; 2018) proposed a generalized form of the complementary function that

136   expresses E/E_{pen} as a sigmoid function (SGC) of E_{rad}/E_{pen}:

137
$$y = \frac{E}{E_{Pen}} = \frac{1}{1 + m \left(\frac{x_{max} - x}{x - x_{min}} \right)^n}$$

138
$$x = \frac{E_{rad}}{E_{Pen}} \qquad (1)$$

139   where x_{max} corresponds to the certain maximum value of x under extremely wet

140   environments, and x_{min} corresponds to the certain minimum value of x under extremely arid

141   environments. In this study, x_{max} and x_{min} were set as 1 and 0, respectively, for convenience.

142   The E_{pen} term is defined by Penman's equation (Penman, 1950; Penman, 1948), which can be

143   expressed as:

144
$$E_{pen} = \frac{\Delta(R_n - G)}{\Delta + \gamma} + \frac{\rho c_p}{\Delta + \gamma} \frac{\kappa^2 u}{ln(\frac{z - d_0}{z_{0m}}) ln(\frac{z - d_0}{z_{0v}})} (e_a{}^* - e_a) \qquad (2)$$

145   where, Δ (kPa C^{-1}) is the slope of the saturation vapor curve at air temperature; R_n is the net

146   radiation; G is the ground heat flux; γ (kPa C^{-1}) is a psychrometric constant; ρ is the air

147   density; c_p is the specific heat; $\kappa = 0.4$ is the von Karman constant; u is the wind speed at

148   measurement height; $e_a{}^*$ and e_a are the saturated and actual vapor pressures of air,

149   respectively; z is the measurement height (Table S1); d_0 is the displacement height; z_{0m} and

150   z_{0v} are the roughness lengths for momentum and water vapor, respectively, which are

151   estimated from the canopy height (h_c, Table S1), $d_0 = 0.67 h_c$, $z_{0m} = 0.123 h_c$, and $z_{0v} =$

152    $0.1 z_{0m}$ (Monin and Obukhov, 1954; Allen et al., 1998). E_{rad} is the radiation term of Penman

153   evaporation:

$$E_{rad} = \frac{\Delta(R_n - G)}{\Delta + \gamma} \tag{3}$$

155

156   The two parameters m and n of equation (1) can be determined by the Priestley-Taylor

157   coefficient α and the asymmetric parameter b (Han and Tian, 2018).

$$\begin{cases} n = 4\alpha(1 + b^{-1})x_{0.5}(1 - x_{0.5}) \\ m = (\frac{x_{0.5}}{1 - x_{0.5}})^n \end{cases} \tag{4}$$

159   where, $x_{0.5}$ is a variable that corresponds to $y = 0.5$ and equals $\frac{0.5 + b^{-1}}{\alpha(1 + b^{-1})}$.

160

2.2 Polynomial generalized complementary function

162   Brutsaert (2015) proposed the polynomial generalized complementary (PGC) function, which

163   describes the relationship between E/E_{pa} and E_{po}/E_{pa}. We uniformed the independent variable

164   as E_{rad}/E_{pen} to compare the two functions conveniently, and the polynomial function can be

165   expressed as:

$$y = (2 - c)\alpha^2 x^2 - (1 - 2c)\alpha^3 x^3 - c\alpha^4 x^4 \tag{5}$$

167   where, c is an adjustable parameter. When $c = 0$, equation (5) reduce to

$$y = 2\alpha^2 x^2 - \alpha^3 x^3 \tag{6}$$

169

2.3 Parameter optimization method

171   Typically, α has a default value of 1.26 (Priestley & Taylor, 1972). Since some studies have

172   shown that a constant α may cause illogical results and biases in estimating E, it is suggested

173   to specify α for diverse scenarios (Hobbins, Ramírez, Brown, & Claessens, 2001; Ma et al.,

174   2015a; Sugita et al., 2001; Szilagyi, 2007). According to the complementary principle, under

10

175   wet conditions, E is close to E_{pen} and the Priestley-Taylor's evaporation ($E_{PT} = \alpha\, E_{rad}$).

176   Specifically, when E/E_{pen} is larger than a threshold (0.9 is commonly adopted), E_{PT} can be

177   considered to be approximately equal to the observed E; thus, α can be calculated by E/E_{rad}

178   (Kahler and Brutsaert, 2006; Ma et al., 2015a). In this study, α was calculated by this method

179   based on the mean value of E/E_{rad} under wet conditions ($E/E_{pen} > 0.9$). When all the E/E_{pen}

180   values are less than 0.9, α was set as the default value of 1.26. The key parameter b in SGC

181   was calibrated by an optimization algorithm with the objective function as the minimization

182   of the mean absolute error (MAE) between the estimated E (by equation (1)) and the

183   observed E. Similarly, the key parameter c in PGC was calibrated by an optimization

184   algorithm with the objective function as the minimization of the MAE between the estimated

185   E (by equation (5)) and the observed E. Since we used the optimization algorithm to

186   determine the parameter b in the SGC function, it is a fair manner to use the optimal c value

187   instead of a constant value ($c = 0$) in the PGC function.

188

189   To make the model parsimonious, we gave one value for the parameters (α, b and c) at each

190   site for every different time scale. If the parameter was alterable, for example, it was monthly

191   dependent, and we would have to calibrate 12 parameters instead of one value for the whole

192   study period. The purpose of this study is to determine the most suitable timescale for the

193   complementary functions, and the variances of the key parameter within a timescale will

194   introduce extra uncertainties. The accuracy will increase when an alterable parameter (that

195   means a higher number of parameters) is used; however, the probability of overfitting risk

196   will increase at the same time. In addition, in comparison to a group of parameters, a general

197   representation of the parameter is more helpful in detecting its overall trend as the change in

198   the timescale.

199

200   **2.4 Data sources and data processing**

201   The eddy flux data analyzed in this study were obtained from the FLUXNET database

202   (http://fluxnet.fluxdata.org, Baldocchi et al., 2001). Observations from a total of 88 sites

203   around the world were analyzed. Detailed information on these sites is listed in Table S1.

204   These sites were selected from the FLUXNET database because they have observations

205   longer than 5 years. The 88 sites include 11 IGBP (International Geosphere-Biosphere

206   Programme) land cover classes: ENF, evergreen needleleaf forests (27 sites); EBF, evergreen

207   broadleaf forests (8); DBF, deciduous broadleaf forests (13); MF, mixed forests (5); OSH,

208   open shrublands (4); CSH, closed shrublands (1); WSA, woody savannas (3); SAV, savannas

209   (4); GRA, grasslands (15); CRO, croplands (6); and WET, permanent wetlands (2). The

210   climates of the 88 sites range from arid to humid. Among the 88 sites, 11 sites have mean

211   annual precipitation levels lower than 200 mm, 47 sites have precipitation levels between 200

212   ~ 500 mm, and 30 sites have precipitation levels above 500 mm. Eleven sites are located in

213   the Southern Hemisphere (i.e., Australia, Brazil, and South Africa) and the others are located

214   in the Northern Hemisphere.

215

216   Variables including net radiation, sensible heat flux, latent heat flux, ground heat flux, wind

217   speed, air temperature, air pressure, precipitation, relative humidity, and vapor pressure

218   deficit were acquired from the daily, weekly, and monthly datasets on the FLUXNET

219   website. We analyzed the observations in the growing seasons from April to September for

220   the Northern Hemisphere and from October to March for the Southern Hemisphere. These

221   study periods were selected to avoid the high biases caused by the low level of solar radiation

222   or extremely low evaporation (≈ 0) during the nongrowing season. The seasonal and annual

223   data were acquired by averaging the monthly data of the growing seasons. Following Ershadi

224   et al. (2014), the energy residual corrected latent heat fluxes were used, which means the

225   residual term in the energy balance is attributed to the latent heat to force the energy balance

226   closure. To investigate the influence of different residual correction methods, the Bowen ratio

227   energy balance method was also adopted in the uncertainty analysis. In the Bowen ratio

228   method, the residual term is attributed to sensible heat and latent heat by preserving the

229   Bowen ratio (Twine et al., 2000). The latent heat, sensible heat, and available energy ($R_n - G$)

230   are restricted to positive values (Han and Tian, 2018). The energy balance residual (W m^{-2})

231   and energy balance closure ratio for each site are shown in Table S1.

232

233   The Nash‑Sutcliffe efficiency (NSE, Legates and McCabe, 1999) is used to evaluate the

234   efficiency of estimating E by the two generalized complementary functions:

$$\text{NSE} = 1 - \frac{\sum(E - E_{est})^2}{\sum(E - \bar{E})^2} \qquad (7)$$

236   where, E_{est} (W m^{-2}) is the estimated evaporation according to equation (1) or equation (5) and

237     $\bar{E}$ is the mean value of E (W m^{-2}).

238

239   **3. Results and discussion**

240   **3.1 Performance of the SGC function at multiple time scales**

241   The relationship between the estimated E_{est} (site mean values) based on the SGC function

242   (equation (1)) and the observed E at the 88 sites at multiple time scales is shown in Figure 1.

243   The regression equations and determination coefficients (R^2) were calculated by the site mean

244   results. Each dot in Figure 1 represents the site mean result averaged by daily (Figure 1a),

245   weekly (Figure 1b), monthly (Figure 1c), and yearly (Figure 1d) results, and the total

246   observation number is 88 (sites) at each timescale. Most of the results are near the 1:1 line,

247   and all the regression slopes are close to 1 with high R^2 (0.95 ~ 0.99), which means the

248   sigmoid function exhibits a good performance in estimating E at multiple time scales. The

249   evaluation merits show that the performance varies at each time scale. The NSE values of the

250   SGC functions for each site at different time scales are listed in Table S2. For the 88 sites,

251   nearly half of the sites (40) have the highest NSE at the monthly scale, 12 sites have the

252   highest NSE at the daily scale, 13 sites have the highest NSE at the weekly scale, and 23 sites

253   have the highest NSE at the annual scale. The mean results of NSE_H, R^2_H, and $RMSE_H$ (the

254   subscript H corresponds to the sigmoid function proposed in Han and Tian, 2018) of these

255   sites are shown in Table 1. R^2_H represents the mean value averaged by the determination

256   coefficients within each site. When the timescale changes from day to month, the mean NSE_H

257   increases from 0.33 to 0.55, and R^2_H also increases from 0.61 to 0.75 (Table 1). However,

258   they both decrease at the annual scale ($NSE_H = 0.18$ and $R^2_H = 0.61$). These results indicate

259   that the SGC function exhibits the highest skill at the monthly scale. We inferred that there is

260   a tradeoff between the random error and the number of observations. $RMSE_H$ values decrease

261   from 24.56 W m^{-2} at the daily scale to 7.33 W m^{-2} at the annual scale, which means that the

262   random error decreases as the time scale increases. At the same time, the fewer observations

263   at the annual scale result in decreased variabilities of x and y, which affect the performance of

264   the SGC function. On the other hand, Morton (1983) did not suggest using the

265   complementary principle for short time intervals (e.g., less than 3 days), mainly considering

266   the lag times associated with heat and water vapor change in the atmosphere, which may

267   provide a possible inference for the weak performance at the daily scale.

268

269   In previous studies, the SGC function was mainly applied at the daily scale. For example, the

270   results of Ma et al. (2015b) in the alpine steppe region showed that the NSE of the sigmoid

271   function is 0.26 at the daily scale, which is lower than our mean value in the grassland (0.73

272   ± 0.08). The RMSE (11.06 W m^{-2}) is smaller than ours (16.36 ± 1.48 W m^{-2}). The mean NSE

273   of the 20 EC sites from FLUXNET is 0.66 at the daily scale in Han and Tian (2018),

274   approximately two times the result in this study, and the RMSE (18.6 ± 0.94 W m^{-2}) is lower

275   than our mean result of 88 sites (24.56 ± 0.95 W m^{-2}).

276

277   The SGC function for the five selected sites of different ecosystem types is shown in Figure 2

278   to show the performance at multiple time scales (red lines in Figure 2). These five EC

279   monitoring sites were selected because they have long-term observations (> 10 years). The

280   five sites include an evergreen needle forest (CA-TP1, Figures 2(a) to (d)), a deciduous broad

281   forest (US-UMB, Figures 2(e) to (h)), a woody savanna (US-SRM. Figures 2(i) to (l)), a

282   cropland (US-Ne2, Figures 2(m) to (p)) and a grassland (US-Wkg, Figures 2(q) to (t)). As

283   observations decrease from the daily to the annual scale, the results converge on the middle

284   part of the sigmoid curves and lie closer to the fitted lines. For some sites, the annual results

285   concentrate on a narrow range with lower annual variabilities (e.g., Figures 2(h), 2(l) & 2(t)).

286   Generally, the key parameter (b) of the SGC function at these sites increases from the daily

287   scale to the annual scale, which indicates that the sigmoid curves in the two-dimensional

288   space of E_{rad}/E_{pen}-E/E_{pen} move upwards. A detailed discussion about the variation in the

289   parameters is provided in Section 3.4.

290

291   **3.2 Performance of the PGC function at multiple time scales**

292   The relationship between the estimated E_{est} (site mean values) based on the PGC function

293   (equation (5)) and the observed E at the 88 sites at multiple time scales is shown in Figure 3.

294   The slopes of the regression increase from 0.9 to 1 as the timescale changes from day to

295   month and further increase to 1.01 at the annual scale. The intercept terms decrease from

296   13.06 W m^{-2} at the daily scale to 0.01 W m^{-2} at the monthly scale and further decrease to

297   −0.25 W m^{-2} at the annual scale. The R^2 values increase from 0.83 to 0.99 as the time scale

298   increases. These coefficients of the regression show that the PGC function exhibits the

299   highest skill at the monthly scale. The NSE values of the PGC functions for each site at

300   different time scales are listed in Table S2. For the 88 sites, 42 sites have the highest NSE at

301   the monthly scale, 7 sites have the highest NSE at the daily scale, 14 sites have the highest

302   NSE at the weekly scale, and 25 sites have the highest NSE at the annual scale. The mean

303   values of NSE$_B$, R^2_B, and RMSE$_B$ (the subscript B corresponds to the polynomial function

304   proposed in Brutsaert, 2015) of these sites are shown in Table 1. When the timescale changes

305   from day to month, NSE$_B$ increases from 0.19 to 0.50, and R^2_B increases from 0.61 to 0.75.

306   They decrease at the annual scale (NSE = 0.25 and R^2_H = 0.63). Again, these evaluation

307   merits indicate that the PGC function also exhibits the highest skill at the monthly scale,

308   which is the same as for the SGC function.

309

310   The PGC function has been applied at multiple time scales in previous studies. Zhang et al.

311   (2017) evaluated the performance of the PGC function in estimating evaporation at 4 EC flux

312   sites located across Australia, and their results showed that the mean RMSE (24.67 W m^{-2})

313   and R^2 (0.65) are close to our results (RMSE = 26.83 ± 1.16 W m^{-2} and R^2 = 0.61) at the

314   daily scale. In Crago and Qualls (2018), the mean RMSE of 7 EC sites at the weekly scale

315   was 20.6 W m^{-2} and the mean R^2 was 0.81, which are close to our mean results (RMSE =

316   19.17 ± 0.95 W m^{-2} and R^2 = 0.7).

317

318   The PGC functions for the five selected sites are also shown in Figure 2 (green lines). The

319   fitted lines are almost the same as those of the SGC function in most situations when x is not

320   too high. However, they diverge from each other when x becomes larger. Finally, y exceeds 1

321   when x is larger than $1/\alpha$. Generally, the key parameter (c) of the PGC function at these sites

322   decreases from the daily scale to the annual scale, which also indicates that the fitted curves

323   move upwards.

324

325   **3.3 Performance comparison of the SGC and PGC functions**

326   The results from the 88 sites (Figure 1, Figure 3 and Table 1) show that the performances of

327   the two functions are similar at monthly and annual time scales, while the SGC function

328   performs slightly better than the PGC function at daily and weekly time scales. According to

17

329   the results in Figure 2, the two functions with calibrated parameters are approximately

330   identical under non-humid environments, but their difference increases as x (E_{rad}/E_{pen})

331   increases. We found that the values of α for all sites are greater than 1.0 in our study, which

332   means that the PGC model cannot work properly under the condition of $1/\alpha < E_{rad}/E_{pen} < 1.0$.

333   At daily and weekly time scales, a substantial number of ecosystems can produce very high

334   E_{rad}/E_{pen} values. Specifically, 63 of the 88 sites have high E_{rad}/E_{pen} values ($x > 1/\alpha$) at the

335   daily scale, and 24 sites have high values at the weekly scale. However, there are only 3 sites

336   with an $x > 1/\alpha$ at the monthly scale, and no site has that value at the yearly scale. For the

337   SGC function, in super humid conditions, the upper part of the sigmoid curve is nearly flat

338   and closer to the observations (e.g., Figures 2 (a), (m) & (n)). However, for the PGC function,

339   theoretically, it cannot be applied when x is over $1/\alpha$ because the estimated E_{est} will be higher

340   than E_{pen}, which is illogical. Thus, the sigmoid function performs slightly better at daily and

341   weekly time scales than the polynomial function. However, the difference vanishes at the

342   monthly scale as few high E_{rad}/E_{pen} values occur.

343

344   According to the results, the performance of the PGC function is more sensitive to the

345   timestep than that of the SGC function. On the one hand, the regression relationship between

346   E_{est} and the observed E of the 88 sites shows that the performance of the SGC function

347   remains more stable (Figure 1), while the regression results of the PGC function have higher

348   variation when the time scale changes (Figure 3). On the other hand, the estimation merits

349   (Table 1) further confirm the sensitivity of the PGC function. From the daily scale to the

350   monthly scale, the increase in NSE_H is 0.22, while the increase in NSE_B is 0.31; $RMSE_H$

351 decreases by 11.36 W m^{-2} (46%), and RMSE$_B$ decreases by 13.13 W m^{-2} (49%). At the daily

352 scale, quite a few ecosystems (63 of 88 sites) can experience frequent high E_{rad}/E_{pen} (> 1/α)

353 values, and the PGC function does not have the ability to simulate E accurately in this

354 situation ($E_{est} > E_{pen}$) resulting in lower efficiency. We have carried out an additional analysis

355 that adopts $E = E_{pen}$ for $1/\alpha < E_{rad}/E_{pen} < 1.0$ in the PGC function, and the resultant NSE$_B$

356 (0.19 vs 0.19) and RMSE$_B$ (26.83 W m^{-2} vs 26.68 W m^{-2}) present very similar results. As the

357 time scale increases, the results converge on the middle part of the fitted line, and the number

358 of high x greatly decreases (Figure 2). Thus, the efficiency of the PGC function obviously

359 increases. This is the reason that the polynomial function acts more sensitive to the timestep.

360

361 In addition, we found that the two complementary functions perform reasonably well at

362 shorter timescales (i.e., day and week) with relatively high R^2 values. Additionally, the

363 estimations of site mean evaporation at shorter timescales are accurate (Figure 1 and Figure

364 3), especially for the SGC function. These results suggest that the generalized complementary

365 functions have the ability to estimate evaporation accurately even at shorter timescales.

366

367 **3.4 Dependence of the key parameters of the SGC and PGC functions on time scales**

368 The key parameters of the two complementary functions (b of the SGC function and c of the

369 PGC function) vary at multiple time scales (Figure 2). To explore their changes, the values of

370 $1/b$ and c at the 88 sites were averaged at each timescale. To take into account the situation in

371 which b is equal to infinity, we used $1/b$ instead of b in this analysis. Figure 4 shows the

372 change in the two complementary functions with varied parameters at multiple time scales.

373   The averaged $1/b$ decreases from 0.45 ± 0.05 at the daily scale to 0.24 ± 0.03 at the annual

374   scale (Figure 4a), and the averaged c decreases from 0.98 ± 0.19 at the daily scale (Figure 4b)

375   to -0.37 ± 0.22 at the annual scale. The sign of c changes from positive to negative at the

376   monthly scale.

377

378   We show the histograms of $1/b$ and c at multiple time scales in Figure 5 and Figure 6,

379   respectively. At the daily scale, half of the $1/b$ values are lower than 0.3, and the mean value

380   is 0.45 ± 0.05. At the weekly scale, the peak of the distribution moves left, and almost half of

381   the $1/b$ values are lower than 0.2 with a mean value of 0.36 ± 0.04. At the monthly scale, the

382   mean value is 0.29 ± 0.04, and the $1/b$ values continue to decrease. At the annual scale, the

383   mean value decreases to 0.24 ± 0.03, and 61% of the $1/b$ values are lower than 0.2. According

384   to Figure 6, at the daily scale, c follows a normal distribution (p-value $= 0.17$, Kolmogorov-

385   Smirnov test) with a mean value of 0.98 ± 0.21. Nearly 1/3 of the c values are lower than 0.

386   At the weekly scale, the center of the distribution moves left with a mean value of $0.43 \pm$

387   0.24. Half of the c values are lower than 0. At the monthly scale, the mean value is $-0.04 \pm$

388   0.23, and 58% of the c values are lower than 0. At the annual scale, the mean value decreases

389   to -0.37 ± 0.25, and 63% of the c values are lower than 0. These results support our

390   conclusion that $1/b$ and c decrease as the time scale increases. Generally, the distribution of

391     $1/b$ and c also moves left within each ecosystem type according to Figures 5 and 6.

392

393   The reduction in $1/b$ and c indicates that the curves of the complementary functions move

394   upwards as the time scale increases. Under non-humid conditions, the sigmoid function is a

20

395 concave function, which means:

$$\frac{1}{2}[f(x_1) + f(x_2)] > f(\frac{x_1 + x_2}{2}) \tag{8}$$

397 where, f is the concave function, and x_1 and x_2 represent any two values on the x-axis. Since

398 most of the results follow the fitted line, the averaged results of the longer timestep will move

399 upwards in the two-dimensional space of E_{rad}/E_{pen}-E/E_{pen}, as well the new fitted curve.

400 Although under super humid conditions, the SGC function is a convex function, there are

401 fewer data under this condition as the time scale increases, and the shape of this part is almost

402 unchanged (Figure 4a). For the PGC function, when x is in the range of 0 to $1/\alpha$, most part of

403 it is a concave function. For example, in the situation where c is equal to 0, the second

404 derivative is higher than 0 as long as x is lower than 2/3.

405

406 Furthermore, we found that the two key parameters b and c present a significant correlation,

407 which provides additional evidence that the two functions can substitute each other in a

408 sense. In other words, the two functions with calibrated parameters substantially provide

409 similar descriptions of the distribution of the results in the state space ($x = E_{rad}/E_{pen}$, y

410 $=E/E_{pen}$). They can covert to each other in most situations since the two functions are

411 generally equivalent to the linear asymmetric function when x is neither excessively large nor

412 excessively small. The relationship can be described as follows: $1/b = 0.01c^2 + 0.11c + 0.24$

413 with R^2 being higher than 0.96 at the monthly scale (Figure 7). The relationship remains at

414 other time scales with a slight difference in the regression coefficients. At the daily scale,

415 when c is equal to 0, the corresponding b is equal to 4.5, which is the same as that of the

416 theoretical derivation in Brutsaert (2015).

417

In this study, the physical meaning of the Priestley-Taylor coefficient α, which represents the

ratio of E_{PT} (the Priestley-Taylor evaporation) and E_{rad} with the default value of 1.26

(Priestley & Taylor, 1972; Brutsaert & Stricker, 1979), was retained. This fundamental

definition of α may result in a smaller range of E_{rad}/E_{pen} in the PGC function. Liu et al. (2016)

suggested that α_e (the calibrated α with $c = 0$) in the PGC function is only a weak analog of

the Priestley-Taylor coefficient, and Brutsaert (2019) directly considered α_e as an adjustable

parameter, which can be equal to or smaller than 1. We added the analysis that c is fixed to 0

and α is calibrated as α_e. This analysis showed that the two methods provide similar results

(mean RMSE $= 14.99$ W m^{-2} for α_e vs 16.67 W m^{-2} for α), and the conclusion of the time

scale issue is consistent by adopting either α or α_e in the analysis. The optimal α_e has a

significantly negative linear relationship with the optimal c and the Pearson correlation

coefficient is -0.8. This scenario suggests that calibrating either of the two parameters (α_e and

c) is equivalent (Han et al., 2012).

3.5 Uncertainty analysis

3.5.1 Influence of ecosystem types

The evaluation merits of the generalized complementary functions may differ among

ecosystem types. However, our results show that such variation generally does not affect our

conclusion that the complementary functions perform best at the monthly scale. We show the

performance of the two functions at multiple timescales for each ecosystem type in Table S3.

Generally, the SGC function and the PGC function perform best at the monthly scale in most

439 ecosystem types (9 of 11) with the highest NSE and R^2, which is consistent with the overall

440 results. The exceptions include a closed shrubland site (CSH, N = 1) and evergreen broadleaf

441 forests (EBF, N = 8), in which the complementary functions do not perform as well as in

442 other ecosystem types. The CSH site (IT-Noe) has the highest NSE_H (0.11) and NSE_B (0.12)

443 at the annual scale. In the EBF group, the highest NSE_H (0.15) and NSE_B (0.03) occur at the

444 weekly scale, but the R^2 values at the weekly scale (R^2_H = 0.64; R^2_B= 0.62) and those at the

445 monthly scale (R^2_H = 0.62; R^2_B = 0.61) are similar. The RMSEs at the weekly scale are 14.95

446 W m^{-2} and 16.08 W m^{-2} for the sigmoid function and polynomial function, respectively, and

447 those values at the monthly scale are 12.36 W m^{-2} ($RMSE_H$) and 12.93 W m^{-2} ($RMSE_B$). We

448 inferred that the abnormal results of these two exceptions are related to the lower NSE values

449 in these ecosystem types. The mean NSE values at multiple time scales of CSH (−0.75) and

450 EBF (−0.66) are negative, while the values of the other ecosystem types are all positive.

451

452 **3.5.2 Performance at the seasonal scale**

453 In consideration of the substantial discrepancy between the monthly results and the annual

454 results, we added an analysis at the seasonal scale, which is between the two timesteps. The

455 relationship between the estimated E_{est} (site mean values) and the observed E of the 88 sites

456 at the seasonal scale is shown in Figure S1. For the SGC function, the regression result at the

457 seasonal scale is similar to that at the monthly scale (Figure S1a and Figure 1c). The values of

458 NSE_H (0.33), R^2_H (0.61), and $RMSE_H$ (10.16 W m^{-2}) at the seasonal scale are between the

459 monthly results and the yearly results (Table 1). For the PGC functions, the regression result

460 at the seasonal scale is extremely close to that at the yearly scale (Figure S1b and Figure 3d).

23

461 The evaluation merits ($NSE_B = 0.31$; $R^2_B = 0.63$; $RMSE_B = 9.94$ W m^{-2}) also range between

462 the monthly results and the yearly results (Table 1). These results indicate that the decline in

463 model efficiency has already occurred at the seasonal scale and support our conclusion that

464 the complementary functions perform best at the monthly scale.

465

466 In addition, we also tested the influence of the different energy balance closure methods. The

467 results based on both the "energy residual" (ER) closure correction (e.g., Ershadi et al., 2014;

468 Han and Tian 2018) and the "Bowen ratio" (BR) closure correction support our conclusion

469 that the generalized complementary functions perform best at the monthly scale (Table S4).

470

471 **4. Conclusions**

472 In this study, evaporation estimations were assessed at 88 EC monitoring sites at multiple

473 time scales (daily, weekly, monthly, and yearly) by using two generalized complementary

474 functions (the SGC function and the PGC function). The performances of the complementary

475 functions at multiple time scales were compared, and the variation in the key parameters at

476 different time scales was explored. The main findings are summarized as follows:

477

478 (1) The sigmoid and polynomial generalized complementary functions exhibit higher skill in

479 estimating evaporation at the monthly scale than at the other evaluated scales. The highest

480 evaluation merits were obtained at this time scale. The accuracy of the complementary

481 functions highly depends on the calculation timestep. The NSE increases from the daily scale

482 (0.26, averaged by NSE_H and NSE_B) to the weekly scale (0.37) and monthly scale (0.53),

483   while it decreases at the seasonal scale (0.32) and the annual scale (0.22). The regression

484   parameters between estimated E_{est} and observed site mean E also support this conclusion for

485   the PGC function. The variations among the different ecosystem types or between different

486   energy balance closure methods generally have no effect on this conclusion. Further

487   evaporation estimation studies with complementary functions can choose the monthly

488   timestep to achieve the most accurate results.

489

490   (2) The SGC function and the PGC function are approximately identical under non-humid

491   environments, while the SGC function performs better under super humid conditions implied

492   by high values of x ($> 1/\alpha$) when the PGC function is theoretically useless ($E_{est} > E_{pen}$). At

493   daily and weekly time scales, a substantial number of ecosystems can experience frequent

494   high x values, and thus, the SGC function performs slightly better than the PGC function at

495   these time scales. However, both functions perform very similarly at monthly and annual

496   time scales with few high x values. In addition, the performance of the PGC function is more

497   sensitive to the timestep than that of the SGC function.

498

499   (3) The key parameter b of the SGC function increases and the key parameter c of the PGC

500   function decreases as the time scale increases. The value of $1/b$ is a quadratic function of c

501   with a higher R^2 (> 0.96). The relationship at the monthly scale can be described as $1/b =$

502    $0.01c^2 + 0.11c + 0.24$. This relationship indicates that the two functions serve as substitutes to

503   some extent.

504

505 In this study, i to determine the most suitable time scale for applying the complementary

506 principle, the key parameters (b and c) were calibrated to achieve the best model performance

507 at each timescale. Further studies on the prognostic application of the complementary

508 principle could focus on the reasonable prediction of the key parameters, and with the

509 predictable flexible parameters at different timescales, the complementary principle could be

510 integrated into hydrological models to reduce the uncertainty associated with evaporation

511 estimations.

512

513 **Code/Data availability**

514 All the data used in this study are from FLUXNET (http://fluxnet.fluxdata.org). The

515 intermediate data are available on request from the corresponding author

516 (tianfq@mail.tsinghua.edu.cn).

517

518 **Author contribution**

519 Songjun Han and Fuqiang Tian designed the experiments and Liming Wang carried them out.

520 Liming Wang developed the model code and performed the simulations. Liming Wang

521 prepared the manuscript with contributions from all co-authors.

522

523 **Competing interests**

524 The authors declare that they have no conflict of interest.

525

526 **Acknowledgements**

531

References

Allen, R. G., Pereira, L. S., Raes, D., Smith, M.: Crop evapotranspiration: Guidelines for computing crop water requirements. FAO irrigation and drainage paper No. 56, Food and Agricultural Organization of the U.N., Rome, Italy, 1998.

Baldocchi, D., Falge, E., Gu, L., Olson, R., Hollinger, D., Running, S. et al.: FLUXNET: A new tool to study the temporal and spatial variability of ecosystem-scale carbon dioxide, water vapor, and energy flux densities. Bull Amer. Meteor. Soc., 82(11), 2415–2434, 2001. https://doi.org/10.1175/1520-0477(2001)082<2415:FANTTS>2.3.CO;2

Bouchet, R. J.: Evapotranspiration réelle et potentielle, signification climatique. IAHS Publ, 62, 134-142, 1963.

Brubaker, K. L., Entekhabi, D.: Analysis of feedback mechanisms in land-atmosphere interaction. Water Resour. Res., 32(5), 1343-1357, 1996. https://doi.org/10.1029/96wr00005

Brutsaert, W.: A generalized complementary principle with physical constraints for land-surface evaporation. Water Resour. Res., 51(10), 8087-8093, 2015. https://doi.org/10.1002/2015wr017720

Brutsaert, W.: Spatial distribution of global landscape evaporation in the early twenty first century by means of a generalized complementary approach. J. Hydrometeorol., 21(2), 287-298, 2019. https://doi.org/10.1175/JHM-D-19-0208.1

Brutsaert, W., Li, W., Takahashi, A., Hiyama, T., Zhang, L., Liu, W. Z.: Nonlinear advection-aridity method for landscape evaporation and its application during the growing season in the southern Loess Plateau of the Yellow River basin. Water Resour. Res., 53(1), 270-282, 2017. https://doi.org/10.1002/2016wr019472

Brutsaert, W., Parlange, M. B.: Hydrologic cycle explains the evaporation paradox. Nature, 396(6706), 30-30, 1998. https://doi.org/ 10.1038/23845

Brutsaert, W., Stricker, H.: Advection-Aridity approach to estimate actual regional evapotranspiration. Water Resour. Res., 15(2), 443-450, 1979. https://doi.org/ 10.1029/WR015i002p00443

Budyko, M.I.: Climate and life (Vol. 508). New York: Academic press, 1974.

Crago, R., Crowley, R.: Complementary relationships for near-instantaneous evaporation. J. Hydrol., 300(1-4), 199-211. https://doi.org/10.1016/j.jhydrol.2004.06.002, 2005.

Crago, R. D., Qualls, R. J.: Evaluation of the generalized and rescaled complementary evaporation relationships. Water Resour. Res., 54(10), 8086-8102, 2018. https://doi.org/10.1029/2018wr023401

Ershadi, A., McCabe, M. F., Evans, J. P., Chaney, N. W., Wood, E. F.: Multi-site evaluation of terrestrial evaporation models using FLUXNET data. Agric. For. Meteorol., 187, 46–61, 2014. https://doi.org/10.1016/j.agrformet. 2013.11.008

Fu, B. P.: On the calculation of the evaporation from land surface (in Chinese), Sci. Atmos. Sin., 5(1), 23 – 31, 1981.

Han, S. J., Hu, H. P., Tian, F. Q.: A nonlinear function approach for the normalized complementary relationship evaporation model. Hydrol. Processes, 26(26), 3973-3981, 2012. https://doi.org/10.1002/hyp.8414

Han, S. J, Hu, H. P., Tian, F. Q.: Evaluating the Advection-Aridity model of evaporation using data from field-sized surfaces of HEIFE. IAHS Publ., 322(2):9-14, 2008.

Han, S. J., Hu, H. P., Yang, D. W., Tian, F. Q.: A complementary relationship evaporation model referring to the Granger model and the advection-aridity model. Hydrol. Processes, 25(13), 2094-2101, 2011. https://doi.org/10.1002/hyp.7960

Han, S. J., Tian, F. Q.: Derivation of a sigmoid generalized complementary function for evaporation with physical constraints. Water Resour. Res., 54(7), 5050-5068, 2018.

575   https://doi.org/10.1029/2017wr021755

576 Han, S., Tian, F.: Complementary principle of evaporation: From original linear relationship to generalized
577   nonlinear functions. Hydrol. Earth Syst. Sci., 24(5), 2269-2285, 2020. https://doi.org/10.5194/hess-24-
578   2269-2020

579 Hobbins, M. T., Ramirez, J. A., Brown, T. C.: The complementary relationship in estimation of regional
580   evapotranspiration: An enhanced Advection-Aridity model. Water Resour. Res., 37(5), 1389-1403,
581   2001. https://doi.org/10.1029/2000wr900359

582 Hobbins, M. T., Ramirez, J. A.: Trends in pan evaporation and actual evapotranspiration across the conterminous
583   U.S.: Paradoxical or complementary? Geophys. Res. Lett. 31.13:405-407, 2004.
584   https://doi.org/10.1029/2004GL019846

585 Hu, Z. Y., Wang, G. X., Sun, X. Y., Zhu, M. Z., Song, C. L., Huang, K. W., Chen, X. P.: Spatial-temporal
586   patterns of evapotranspiration along an elevation gradient on Mount Gongga, Southwest China. Water
587   Resour. Res., 54(6), 4180-4192, 2018. https://doi.org/10.1029/2018wr022645

588 Kahler, D. M., Brutsaert, W.: Complementary relationship between daily evaporation in the environment and
589   pan evaporation. Water Resour. Res, 42(5), 2006. https://doi.org/10.1029/2005WR004541

590 Legates D. R., Mccabe G. J.: Evaluating the use of "goodness-of-fit" Measures in hydrologic and hydroclimatic
591   model validation. Water Resour. Res., 35(1):233-241, 1999. https://doi.org/10.1029/1998wr900018

592 Liu, X. M., Liu, C. M., Brutsaert, W.: Regional evaporation estimates in the eastern monsoon region of China:
593   Assessment of a nonlinear formulation of the complementary principle. Water Resour. Res., 52(12),
594   9511-9521, 2016. https://doi.org/10.1002/2016wr019340

595 Ma, N., Szilagyi, J., Zhang, Y., Liu, W.: Complementary relationship-based modeling of terrestrial
596   evapotranspiration across China during 1982–2012: Validations and spatiotemporal analyses. J.
597   Geophys. Res. Atmos., 124, 4326–4351, 2019. https://doi.org/10.1029/2018JD029850

598 Ma, N., Zhang, Y. S., Szilagyi, J., Guo, Y. H., Zhai, J. Q., Gao, H. F.: Evaluating the complementary relationship
599   of evapotranspiration in the alpine steppe of the Tibetan Plateau. Water Resour. Res., 51(2), 1069-1083,
600   2015a. https://doi.org/10.1002/2014wr015493

601 Ma, N., Zhang, Y. S., Xu, C. Y., Szilagyi, J.: Modeling actual evapotranspiration with routine meteorological
602   variables in the data-scarce region of the Tibetan Plateau: Comparisons and implications. J. Geophys.
603   Res. Biogeosci., 120(8), 1638-1657, 2015b. https://doi.org/10.1002/2015jg003006

604 Monin, A., Obukhov, A.: Basic laws of turbulent mixing in the surface layer of the atmosphere. Contrib.
605   Geophys. Inst. Acad. Sci. USSR, 151(163), e187, 1954.

606 Monteith, J. L.: Evaporation and environment (pp. 205-234): Paper presented at the Symposia of the society for
607   experimental biology. Cambridge University Press (CUP) Cambridge, 1965.

608 Morton, F. I.: Operational estimates of areal evapo-transpiration and their significance to the science and
609   practice of hydrology. J. Hydrol., 66(1-4), 1-76, 1983. https://doi.org/10.1016/0022-1694(83)90177-4

610 Neelin, J. D., Held, I. M., Cook, K. H.: Evaporation-wind feedback and low-frequency variability in the tropical
611   atmosphere. J. Atmos. Sci., 44(16), 2341-2348, 1987. https://doi.org/ 10.1175/1520-
612   0469(1987)044<2341:Ewfalf>2.0.Co;2

613 Parlange, M. B., Katul, G. G.: An advection-aridity evaporation model, Water Resour. Res., 28, 127-132, 1992.
614   https://doi.org/10.1029/91WR02482

615 Penman, H. L.: The dependence of transpiration on weather and soil conditions. J. Soil Sci., 1(1), 74-89, 1950.
616   https://doi.org/10.1111/j.1365-2389.1950.tb00720.x

617 Penman, H. L.: Natural evaporation from open water, bare soil and grass. Proc. R. Soc. London, Ser. A.,
618   193(1032), 120-145, 1948. https://doi.org/10.1098/rspa.1948.0037

619 Priestley, C. H. B., Taylor, R. J.: On the assessment of surface heat-flux and evaporation using large-scale
620   parameters. Mon. Weather Rev., 100(2), 81-92, 1972. https://doi.org/10.1175/1520-
621   0493(1972)100<0081:Otaosh>2.3.Co;2

622 Qualls, R. J., Gultekin, H.: Influence of components of the advection-aridity approach on evapotranspiration
623   estimation. J. Hydrol., 199(1-2), 3-12, 1997. https://doi.org/10.1016/S0022-1694(96)03314-8

624 Shukla, J., Mintz, Y.: Influence of land-surface evapo-transpiration on the earths climate. Science, 215(4539),
625   1498-1501, 1982. https://doi.org/10.1126/science.215.4539.1498

626 Sugita, M., Usui, J., Tamagawa, I., & Kaihotsu, I.: Complementary relationship with a convective boundary
627   layer model to estimate regional evaporation. Water Resources Research, 37(2), 353-365, 2001.
628   https://doi.org/10.1029/2000wr900299

629 Szilagyi, J.: On the inherent asymmetric nature of the complementary relationship of evaporation. Geophysical
630   Research Letters, 34(2), L02405, 1-6, 2007. https://doi.org/10.1029/2006gl028708

631 Twine, T. E., Kustas, W. P., Norman, J. M., Cook, D. R., Houser, P., Meyers, T. P., Wesely, M. L.: Correcting
632   eddy-covariance flux underestimates over a grassland. Agric. For. Meteorol., 103(3), 279-300, 2000.
633   https://doi.org/10.1016/S0168-1923(00)00123-4

634 Wang, K. C., Dickinson, R. E.: A review of global terrestrial evapotranspiration: observation, modeling,
635   climatology, and climatic variability. Rev. Geophys., 50, 2012. https://doi.org/10.1029/2011rg000373

636 Wang, L.M., Tian, F. Q., Han, S. J., Wei, Z. W.: Determinants of the asymmetric parameter in the generalized
637   complementary principle of evaporation. Water Resour. Res, 2020, 56, e2019WR026570.
638   https://doi.org/10.1029/2019WR026570

639 Zhang, L., Cheng, L., Brutsaert, W.: Estimation of land surface evaporation using a generalized nonlinear
640   complementary relationship. J. Geophys. Res. Atmos., 122(3), 1475-1487, 2017.
641   https://doi.org/10.1002/2016jd025936

642 Zhou, H., Han, S., Liu, W.: Evaluation of two generalized complementary functions for annual evaporation
643   estimation on the loess plateau, china. J. Hydrol., 587, 124980, 2020.
644   https://doi.org/10.1016/j.jhydrol.2020.124980
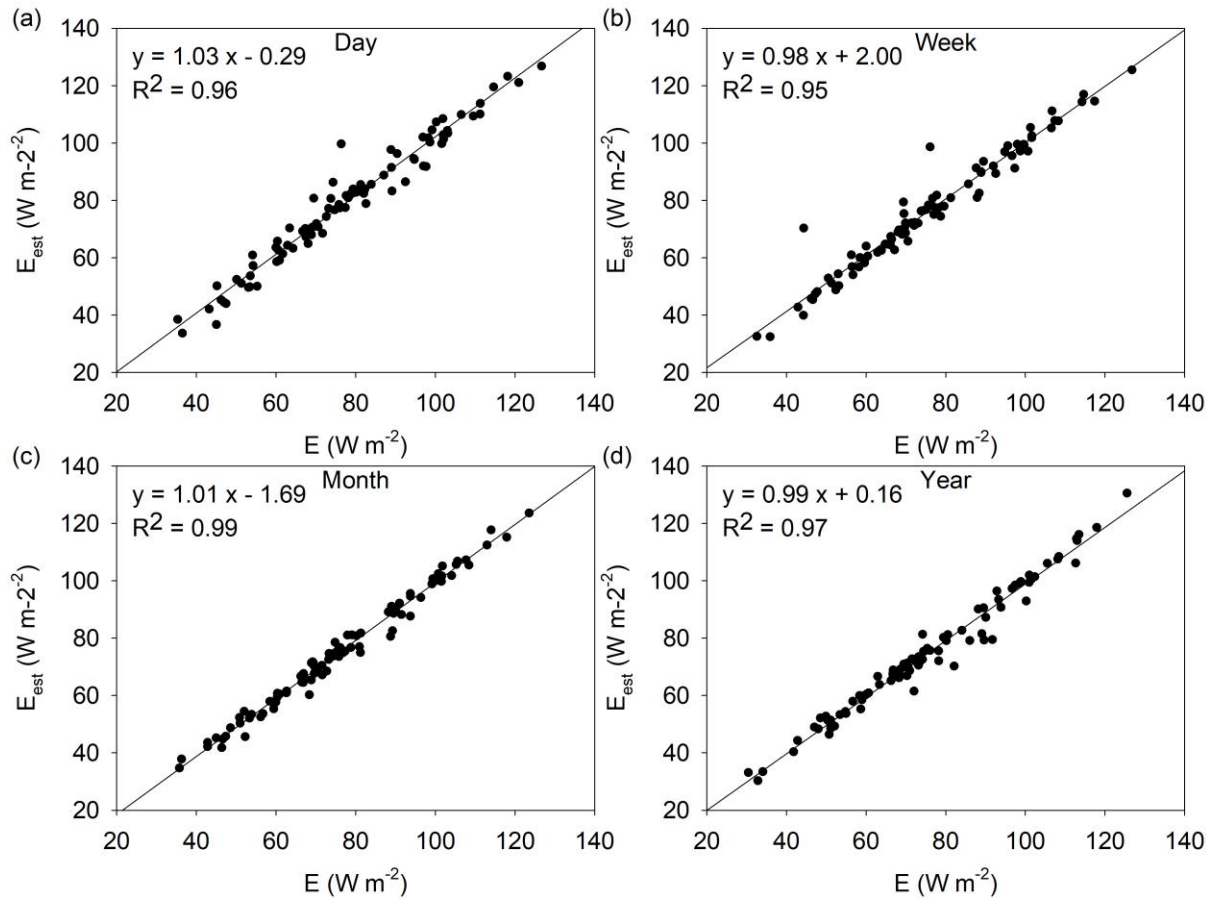
645

List of Figure Captions

Figure 1. The estimated evaporation based on the SGC function (equation (1)) vs the observed site mean evaporation at the daily scale (a), weekly scale (b), monthly scale (c) and yearly scale (d). Each dot represents the site mean result (N = 88 in each panel). The regression equations and determination coefficients (R^2) were calculated by the site mean results of the 88 EC sites.

Figure 2. Plots of E/E_{pen} with respect to E_{rad}/E_{pen} for five selected sites at multiple time scales. The black dots represent the observations; the red lines represent the SGC function; the green lines represent the PGC function; the blue lines are the P-T and Penman boundary lines. ENF, evergreen needleleaf forests; DBF, deciduous broadleaf forests; WSA, woody savannas; CRO, croplands; GRA, grasslands.

Figure 3. As in Figure 1 except for PGC function (equation (5)).

Figure 4. Plots of the SGC equation (1) with $\alpha = 1.26$ and varying $1/b$ values at multiple time scales (a). Plots of the PGC equation (5) with $\alpha = 1.26$ and varying c values at multiple time scales (b). The blue lines are the P-T and Penman boundary lines.

Figure 5. Distribution of the key parameter $1/b$ at daily scale (a), weekly scale (b), monthly scale (c) and yearly scale (d): EBF, evergreen broadleaf forests (8); ENF, evergreen needleleaf forests (27); DBF, deciduous broadleaf forests (13); MF, mixed forests (5); Shrub (12), closed shrubland, open shrublands, woody savannas and savannas; CRO, croplands (6); WET, permanent wetlands (2).

Figure 6. Distribution of the key parameter c at daily scale (a), weekly scale (b), monthly scale (c) and yearly scale (d): EBF, evergreen broadleaf forests (8); ENF, evergreen

31

needleleaf forests (27); DBF, deciduous broadleaf forests (13); MF, mixed forests (5); Shrub

(12), closed shrubland, open shrublands, woody savannas and savannas; CRO, croplands (6);

WET, permanent wetlands (2).

Figure 7. Relationships between $1/b$ and c at the monthly scale.

Table 1. The evaluation merits (NSE, R^2 and RMSE in W m^{-2}) of the two generalized complementary functions using the "energy residual" (ER) closure correction method. The subscript H and B correspond to the SGC function proposed in Han and Tian (2018) and the PGC function proposed in Brutsaert (2015), respectively.

	Day	Week	Month	Season	Year
NSE_H	0.33	0.44	0.55	0.33	0.18
NSE_B	0.19	0.3	0.50	0.31	0.25
R^2_H	0.62	0.7	0.74	0.61	0.61
R^2_B	0.61	0.7	0.75	0.63	0.63
$RMSE_H$	24.56	17.67	13.20	10.16	7.33
$RMSE_B$	26.83	19.17	13.70	9.94	6.96

Figure 1. The estimated evaporation based on the SGC function (equation (1)) vs the observed site mean evaporation at the daily scale (a), weekly scale (b), monthly scale (c) and yearly scale (d). Each dot represents the site mean result (N = 88 in each panel). The regression equations and determination coefficients (R^2) were calculated by the site mean results of the 88 EC sites.
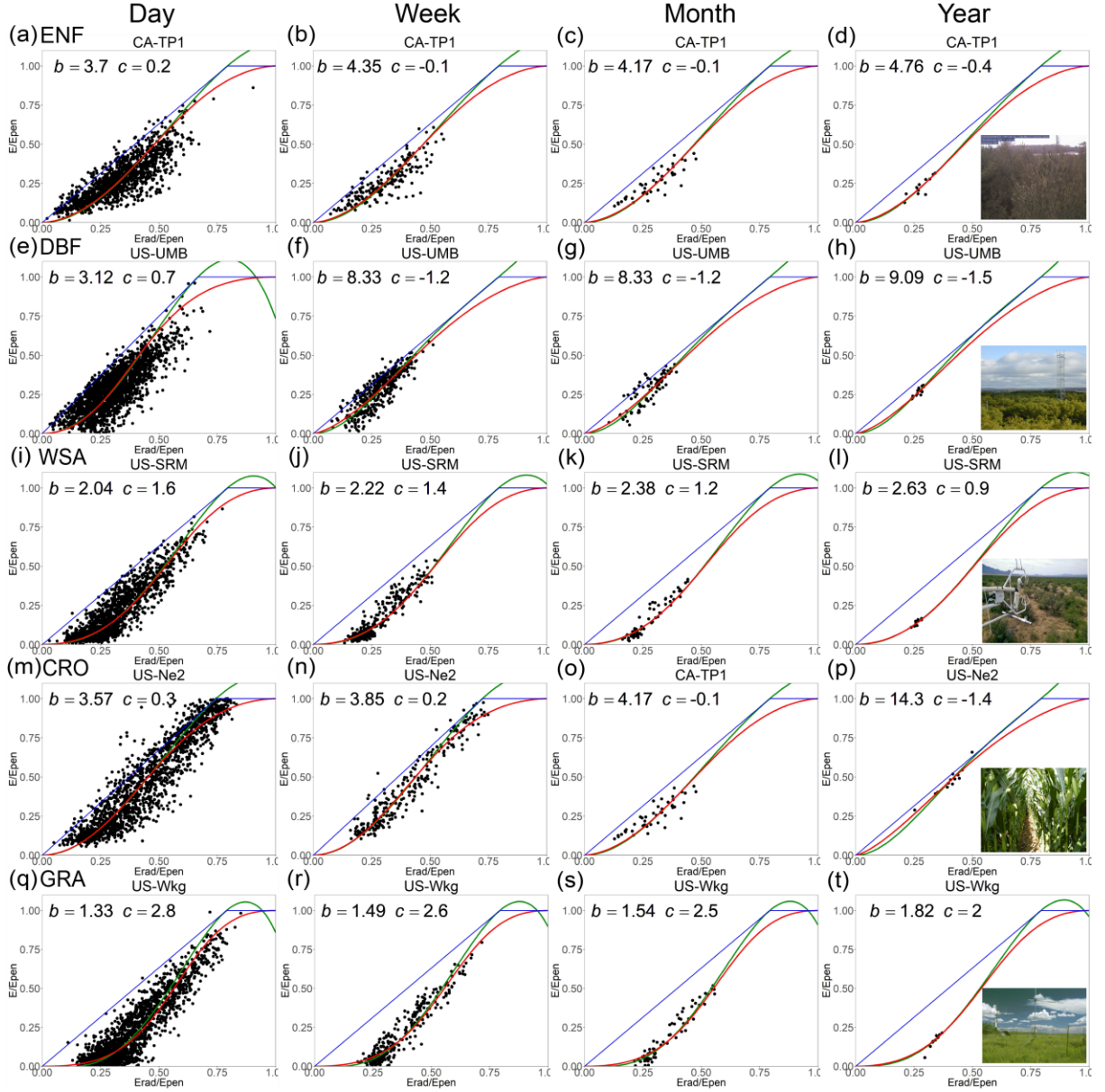
Figure 2. Plots of E/E_{pen} with respect to E_{rad}/E_{pen} for five selected sites at multiple time scales. The black dots represent the observations; the red lines represent the SGC function; the green lines represent the PGC function; the blue lines are the P-T and Penman boundary lines. ENF, evergreen needleleaf forests; DBF, deciduous broadleaf forests; WSA, woody savannas; CRO, croplands; GRA, grasslands.
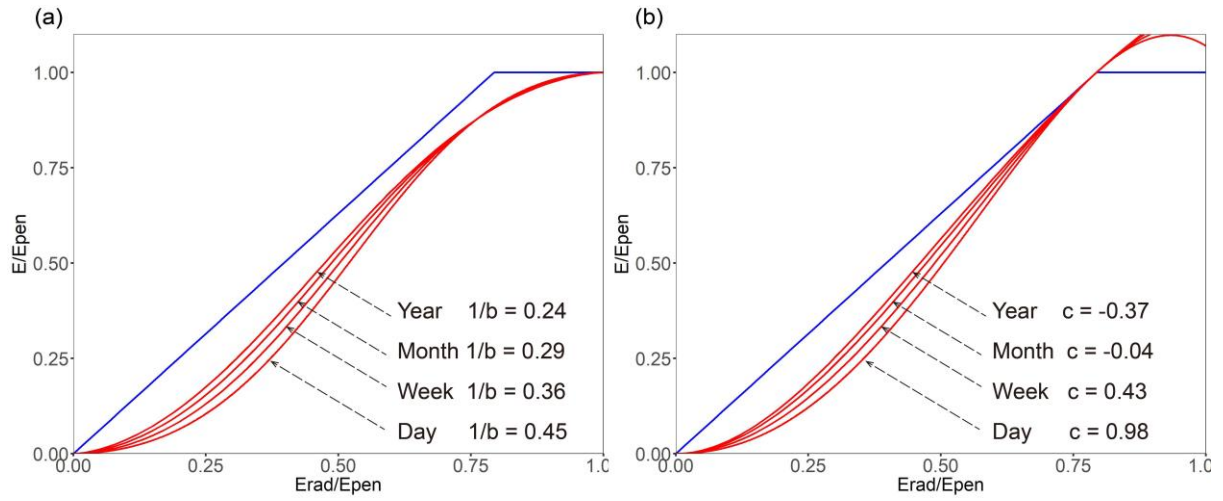
Figure 3. As in Figure 1 except for PGC function (equation (5)).

Figure 4. Plots of the SGC equation (1) with $\alpha = 1.26$ and varying $1/b$ values at multiple time scales (a). Plots of the PGC equation (5) with $\alpha = 1.26$ and varying c values at multiple time scales (b). The blue lines are the P-T and Penman boundary lines.
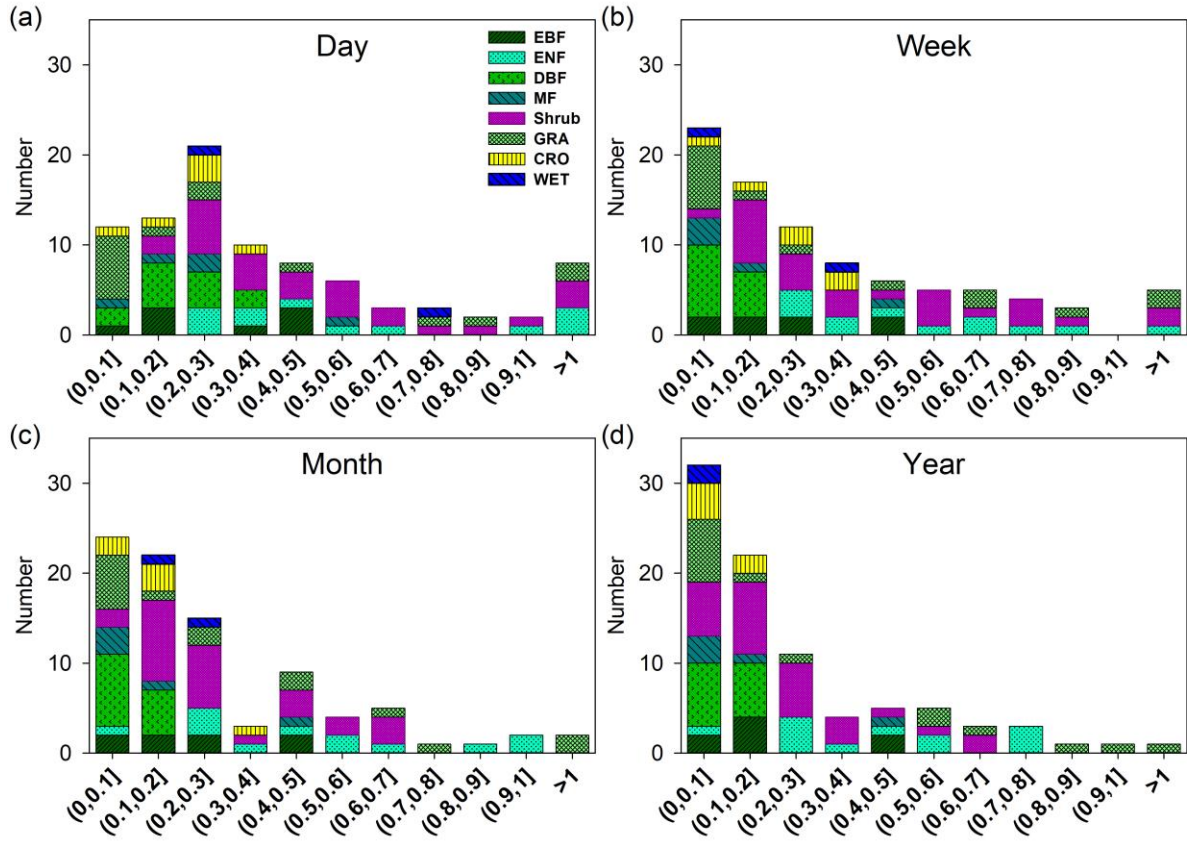
Figure 5. Distribution of the key parameter $1/b$ at daily scale (a), weekly scale (b), monthly scale (c) and yearly scale (d): EBF, evergreen broadleaf forests (8); ENF, evergreen needleleaf forests (27); DBF, deciduous broadleaf forests (13); MF, mixed forests (5); Shrub (12), closed shrubland, open shrublands, woody savannas and savannas; CRO, croplands (6); WET, permanent wetlands (2).
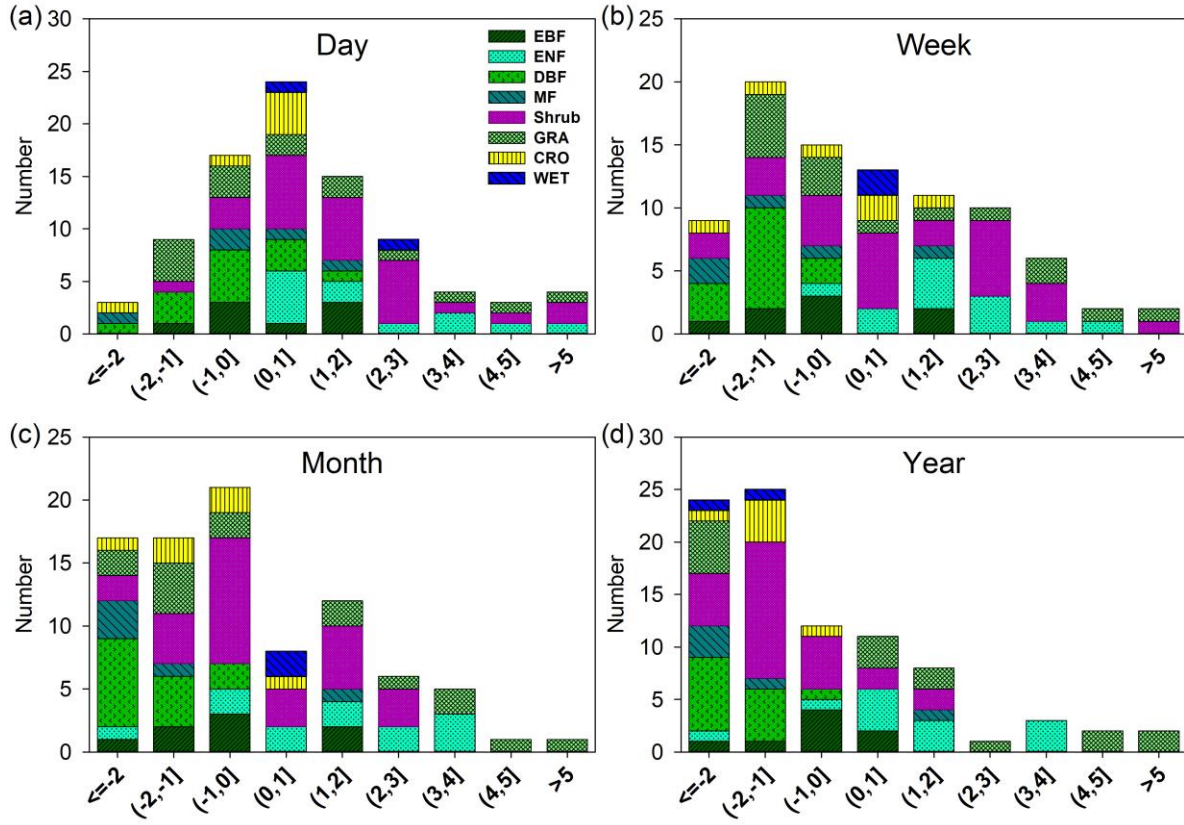
Figure 6. Distribution of the key parameter c at daily scale (a), weekly scale (b), monthly scale (c) and yearly scale (d): EBF, evergreen broadleaf forests (8); ENF, evergreen needleleaf forests (27); DBF, deciduous broadleaf forests (13); MF, mixed forests (5); Shrub (12), closed shrubland, open shrublands, woody savannas and savannas; CRO, croplands (6); WET, permanent wetlands (2).
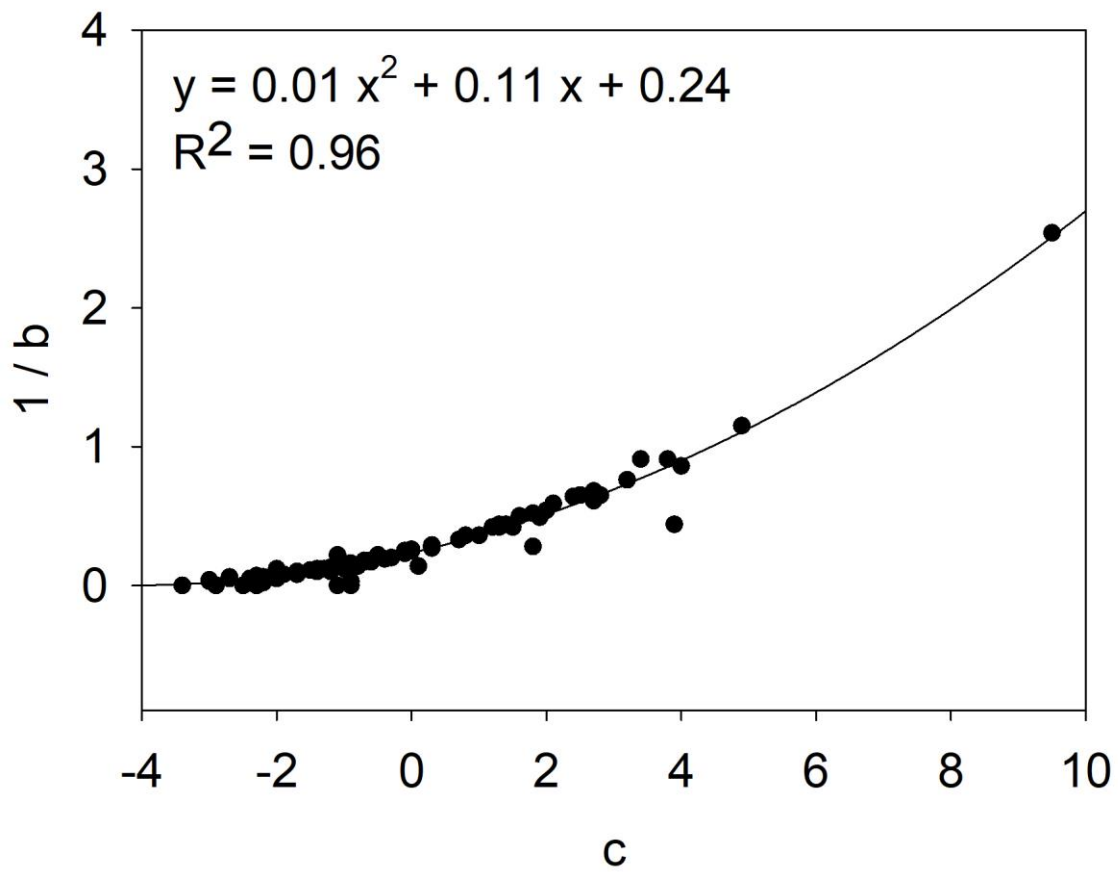
Figure 7. Relationships between $1/b$ and c at the monthly scale.